Published in final edited form as:

ACS Biomater Sci Eng. 2020 November 09; 6(11): 6309–6320. doi:10.1021/acsbiomaterials.0c00942.

Cardiac Stromal Cell Patch Integrated with Engineered Microvessels Improves Recovery from Myocardial Infarction in Rats and Pigs

Teng Su[#],
Joint Department of Biomedical Engineering, University of North Carolina at Chapel Hill and North Carolina State University, Raleigh, North Carolina 27695, United States; Department of Molecular Biomedical Sciences and Comparative Medicine Institute, North Carolina State University, Raleigh, North Carolina 27607, United States;

Ke Huang[#],
Joint Department of Biomedical Engineering, University of North Carolina at Chapel Hill and North Carolina State University, Raleigh, North Carolina 27695, United States; Department of Molecular Biomedical Sciences and Comparative Medicine Institute, North Carolina State University, Raleigh, North Carolina 27607, United States

Kyle G. Mathews,
Department of Clinical Sciences, North Carolina State University, Raleigh, North Carolina 27607, United States

Valery F. Scharf,
Department of Clinical Sciences, North Carolina State University, Raleigh, North Carolina 27607, United States

Shiqi Hu,
Department of Molecular Biomedical Sciences and Comparative Medicine Institute, North Carolina State University, Raleigh, North Carolina 27607, United States

Zhenhua Li,
Department of Molecular Biomedical Sciences and Comparative Medicine Institute, North Carolina State University, Raleigh, North Carolina 27607, United States

Corresponding Author: Ke Cheng – Joint Department of Biomedical Engineering, University of North Carolina at Chapel Hill and North Carolina State University, Raleigh, North Carolina 27695, United States; Department of Molecular Biomedical Sciences and Comparative Medicine Institute, North Carolina State University, Raleigh, North Carolina 27607, United States; Divison of Pharmacoengineering and Molecular Pharmaceutics, Eshelman School of Pharmacy, University of North Carolina at Chapel Hill, Chapel Hill, North Carolina 27599, United States; ke_cheng@ncsu.edu, ke_cheng@unc.edu.

Author Contributions

T.S. and K.H. contributed equally to this work. T.S., M.A.D., K.C., and F.S.L. conceived and designed the study; T.S., K.H., K.G.M., V.F.S., S.H., Z.L., B.N.F., J.C., P.U.D., and M.A.D. performed all of the experiments and collected data; T.S., K.H., M.A.D., K.C., and F.S.L. analyzed the data and wrote the paper.

Complete contact information is available at: https://pubs.acs.org/10.1021/acsbiomaterials.0c00942

Supporting Information

The Supporting Information is available free of charge at https://pubs.acs.org/doi/10.1021/acsbiomaterials.0c00942.
Cell derivation and culture; BMV construction and characterization; echocardiographic and electrocardiographic studies; Masson's trichrome staining; assessment of porcine kidney and liver function; and immunohistochemical assessment of CD3, CD8, CD68, Ki67, and CD34 expression, respectively, as well as cellular apoptosis in the infarcted porcine myocardium after different treatments (PDF)

The authors declare no competing financial interest.

Brianna N. Frame,
Division of Cardiothoracic Surgery, University of North Carolina at Chapel Hill, Chapel Hill, North Carolina 27599, United States

Jhon Cores,
Joint Department of Biomedical Engineering, University of North Carolina at Chapel Hill and North Carolina State University, Raleigh, North Carolina 27695, United States; Department of Molecular Biomedical Sciences and Comparative Medicine Institute, North Carolina State University, Raleigh, North Carolina 27607, United States

Phuong-Uyen Dinh,
Department of Molecular Biomedical Sciences and Comparative Medicine Institute, North Carolina State University, Raleigh, North Carolina 27607, United States

Michael A. Daniele,
Joint Department of Biomedical Engineering, University of North Carolina at Chapel Hill and North Carolina State University, Raleigh, North Carolina 27695, United States; Department of Electrical and Computer Engineering, North Carolina State University, Raleigh, North Carolina 27695, United States;

Frances S. Ligler,
Joint Department of Biomedical Engineering, University of North Carolina at Chapel Hill and North Carolina State University, Raleigh, North Carolina 27695, United States;

Ke Cheng
Joint Department of Biomedical Engineering, University of North Carolina at Chapel Hill and North Carolina State University, Raleigh, North Carolina 27695, United States; Department of Molecular Biomedical Sciences and Comparative Medicine Institute, North Carolina State University, Raleigh, North Carolina 27607, United States; Divison of Pharmacoengineering and Molecular Pharmaceutics, Eshelman School of Pharmacy, University of North Carolina at Chapel Hill, Chapel Hill, North Carolina 27599, United States;

[#] These authors contributed equally to this work.

Abstract

The vascularized cardiac patch strategy is promising for ischemic heart repair after myocardial infarction (MI), but current fabrication processes are quite complicated. Vascularized cardiac patches that can promote concurrent restoration of both the myocardium and vasculature at the injured site in a large animal model remain elusive. The safety and therapeutic benefits of a cardiac stromal cell patch integrated with engineered biomimetic microvessels (BMVs) were determined for treating MI. By leveraging a microfluidic method employing hydrodynamic focusing, we constructed the endothelialized microvessels and then encapsulated them together with therapeutic cardiosphere-derived stromal cells (CSCs) in a fibrin gel to generate a prevascularized cardiac stromal cell patch (BMV–CSC patch). We showed that BMV–CSC patch transplantation significantly promoted cardiac function, reduced scar size, increased viable myocardial tissue, promoted neovascularization, and suppressed inflammation in rat and porcine MI models, demonstrating enhanced therapeutic efficacy compared to conventional cardiac stromal cell patches. BMV–CSC patches did not increase renal and hepatic toxicity or exhibit

immunogenicity. We noted a significant increase in endogenous progenitor cell recruitment to the peri-infarct region of the porcine hearts treated with BMV–CSC patch as compared to those that received control treatments. These findings establish the BMV–CSC patch as a novel engineered-tissue therapeutic for ischemic tissue repair.

Graphical Abstract

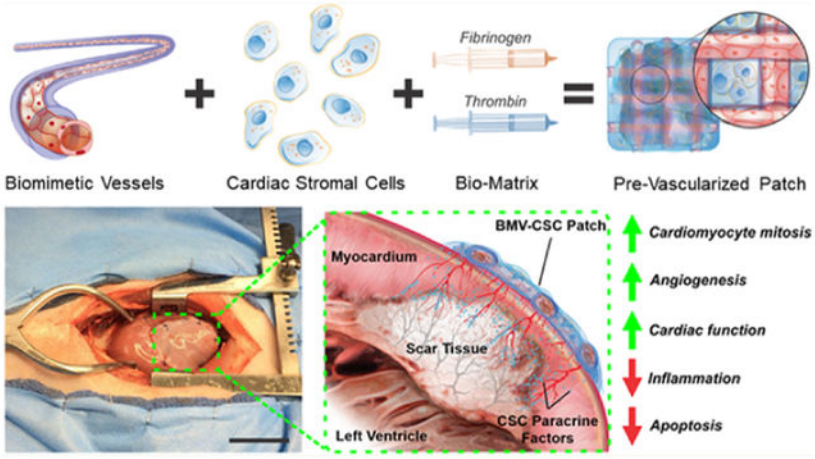

Keywords

microfluidics; cardiac patch; cardiac stromal cells; myocardial infarction; porcine model

INTRODUCTION

Ischemic heart disease contributes to most deaths globally, taking more than 10 million lives each year. After a myocardial infarction (MI), the impaired vasculature and massive cardiomyocyte death concurrent with a profound inflammatory response at the site of ischemia result in physical and physiological changes that give rise to adverse tissue remodeling and functional deterioration.[1,2] Improved growth of new blood vessels and regeneration of myocardial tissue is essential in the treatment of MI to mitigate the heart's insufficient access to nutrients and oxygen due to diseased vasculature and ameliorate dysfunction due to pathological tissue remodeling following MI.[3,4]

Stem cells offer clinical benefits for heart repair after ischemic injury. However, several issues persist that limit therapeutic efficacy, including an extremely low rate of cell lodging in the ischemic myocardium post-transplantation.[5–7] The cardiac patch strategy can effectively localize the therapeutic cell transplants to the scar tissue and promote myocardial regeneration. Recent examples of these cardiac patches include three-dimensional (3D)-printed scaffolds embedded with stem cells, endothelial cell sheet-derived vascularized cardiac patches, and microneedle cardiac patches.[8–10] However, the fabrication of these complex cardiac patches is relatively cumbersome. In addition, cardiac patches that can promote concurrent restoration of both cardiac muscle and blood supply at the injured site in a large animal model remain elusive.

We recently developed a facile modular approach to a prevascularized cardiac patch. Free-standing biomimetic microvessels (BMVs) were constructed using microfluidic hydrodynamic focusing to include human endothelial cells which expanded to confluence in a preculture step, lining the luminal surface.[11,12] Unlike previous strategies, we encapsulated microengineered endothelialized microvessels in a fibrin gel spiked with therapeutic cardiosphere-derived stromal cells (CSCs) to form the vascularized cardiac stromal cell patch (BMV–CSC patch) with dimensions appropriate for rodent studies. We confirmed that the resulting patch sustainably released cardioprotective factors secreted by the CSCs for at least 2 weeks and induced remarkable in vivo cardiomyocyte mitosis and angiogenesis in the post-MI rat hearts.[11]

In this report, we developed the BMV–CSC patches with small (5 mm × 5 mm × 1 mm) and clinically relevant (5 cm × 5 cm × 1 mm) dimensions and tested their therapeutic benefits in rat and pig models of MI. We showed that the BMV–CSC patch therapy promoted cardiac function recovery and limited pathological ventricular remodeling post-MI injury. We also documented an increase in cardiomyocyte proliferating, new blood vessel formation, endogenous progenitor cell activation, and alleviation of proinflammatory cytokine expression. In particular, we showed that the transplantation of the BMV–CSC patch is safe and efficacious in the post-MI heart of immunocompetent pigs, which is favorable for its practical application in the treatment of ischemic heart injury.

EXPERIMENTAL SECTION

Materials.

All chemicals were analytical grade reagents or of the highest purity commercially available and were used as received unless otherwise stated.

Culture of Human Cardiosphere-Derived Stromal Cells (hCSCs).

The hCSCs were derived and cultured according to the previous protocol; the details are provided in the online Supporting Information.[13–16]

BMV–CSC Patch Generation.

The details on the construction of BMVs via hydrodynamic focusing and their characterization are supplied in the online Supporting Information. Prior to testing BMV–CSC patches in an experimental rat MI model, the BMVs were cultured for 2 weeks followed by biaxial arrangement in a 12-well plate, as documented in detail in our prior publication.[11] A Tisseel fibrin gel solution (Baxter) containing fibrinogen (37 mg mL^{-1}), thrombin (217 U mL^{-1}), aprotinin (1270 U mL^{-1}), and hCSCs (8.0×10^6 cells mL^{-1}) was incubated with the above BMVs at 37 °C until complete solidification. The resulting gel disk was cut into squares to generate the BMV–CSC patch (length (mm) × width (mm) × depth (mm), 5 × 5 × 1), with each patch containing six 5 mm long BMVs in a crisscross arrangement and 2.0×10^5 hCSCs. For the HUVEC–CSC patch construction, the microfabricated endothelialized microvessels in the above gel were replaced with an equivalent amount of human umbilical vein endothelial cells (HUVECs; 3.96×10^6 cells mL^{-1}). The CSC patch was constructed using the same procedure except that no BMVs or

HUVECs were added. Each HUVEC–CSC patch contained 9.9×10^4 HUVECs and 2.0×10^5 hCSCs, while each CSC patch contained 2.0×10^5 hCSCs. The empty patch was made of native fibrin gel without any cells. The above cell-laden patches were cultured in a combination of HUVEC and CSC growth media (1:1 mixture) for 8 days before transplantation to the infarcted rat hearts.

For BMV–CSC patch to be tested in the porcine MI model, the fibrin gel solution consisting of fibrinogen (37 mg mL^{-1}), hCSCs (2.0×10^6 cells mL^{-1}), thrombin (217 U mL^{-1}), and aprotinin (1270 U mL^{-1}) was swiftly poured into a square, in-house-made, glass-bottom mold that contained eight 5 cm long BMVs biaxially arranged on the bottom surface. The resulting BMV–CSC patch (length (mm) × width (mm) × depth (mm), 50 × 50 × 1) was incubated at 37 °C until complete solidification. The HUVEC–CSC patch was constructed with an identical size but with the endothelialized microvessels being replaced with an equivalent amount of HUVECs (5.28×10^5 cells mL^{-1}) in the above fibrin gel. A JEOL JSM-7600 field emission scanning electron microscope (JEOL) equipped with a Gatan Alto-2500 cryogenic system (Gatan) was used to assess the patch morphology. The release of regenerative HGF and VEGF for at least 2 weeks from the patch was determined via enzyme-linked immunosorbent assay (ELISA) as documented in our prior publication.[11]

Rat Model of MI.

All animal procedures conform to the protocols of the Institutional Animal Care and Use Committee at North Carolina State University. Briefly, athymic nude rats (female, 5–7 weeks old, 200–250 g, Charles River) were subjected to anesthesia and ventilation to allow surgical MI induction via a permanent occlusion of the left anterior descending (LAD) coronary artery. Afterward, animals were randomized to receive an epicardially sutured BMV–CSC, HUVEC–CSC, CSC, or empty patch. The animals that received left thoracotomy with LAD ligation (MI-only group) and without LAD ligation (sham group) were negative and positive controls, respectively. Four weeks after different treatments, all animals were euthanized for further analysis.

Patch Transplantation in a Porcine Model of MI.

Experimental acute MI was inducted in immunocompetent Yorkshire pigs (female, 8–10 weeks old, 20–30 kg) by permanent LAD occlusion. Briefly, animals were tranquilized with a telazol–ketamine–xylazine cocktail (TKX, 1 mL per 20 kg animal, intramuscular route). Then, animals were intubated and anesthetized via inhalation of a 3% isoflurane–oxygen mixture at an infusion rate of 5–10 $\mu g\ kg^{-1}\ h^{-1}$ (i.e., an hourly dose of the anesthetic gas mixture at 5–10 μg of isoflurane per kilogram of each animal's body weight). A surgical MI was created by distal occlusion of the LAD, followed by epicardial suturing a piece of BMV–CSC or HUVEC–CSC patch to cover the infarct. The control animals received only LAD occlusion without patch treatment (MI-only group). The direction and magnitude of electrical activity generated by the depolarization and repolarization of porcine hearts were recorded pre-MI, 24 h, 2 weeks, and 4 weeks post-MI using a three-lead digital electrocardiograph coupled with an anesthesia monitor (Datascope Passport V Patient Monitor, Mindray). A blood level of cardiac troponin I (cTnI) was measured at the above

time intervals. All animals were euthanized after end point echocardiography 4 weeks post-MI, followed by heart harvest for subsequent morphometrical and histological studies.

Immunohistochemistry Assessment.

Briefly, porcine heart cryosections were subjected to incubation with primary antibodies for detecting Ki67, sarcomeric α-actinin (α-SA), von Willebrand Factor (vWF), phospho-histone H3 (pH3), fetal liver kinase-1 (Flk-1), Nkx2.5, Aurora B kinase (AURKB), CD34, or smooth muscle α-actin (α-SMA). Afterward, samples were incubated with fluorescently conjugated secondary antibodies, followed by counterstain with 4′,6-diamidino-2-phenylindole (DAPI), and then visualization under a Zeiss LSM 710 confocal microscope. A complete list of primary and secondary antibodies employed in this study is supplied in Table S2. To quantify apoptotic cells, terminal deoxynucleotidyl transferase dUTP nick end labeling (TUNEL) staining was performed, followed by counterstain with DAPI and then visualization with confocal microscopy. Five sections were randomly selected and quantified for each animal.

Immunogenicity Studies on BMV–CSC Patch Transplantation.

To assess the cytokine secretion in response to the transplantation of different cardiac patches to the infarcted porcine heart over the entire study period, porcine serum samples were collected pre-MI, 1 h, 24 h, 14 days, and 28 days after MI induction, respectively. Serum levels of IL-1β, IL-6, TNF-α, and IL-10 were quantified via ELISA. In addition, immunohistochemistry was performed using the primary antibodies to detect CD3, CD8, or CD68. Subsequently, samples were incubated with fluorescently conjugated secondary antibodies, followed by staining with DAPI and then visualization with confocal microscopy.

Statistics.

All values were represented as mean ± standard deviation (SD) or Tukey box and whisker plots of a least three independent assays. A p-value less than 0.05 denotes statistical significance between two data groups assessed via a two-tailed unpaired Student's t-test or across three or more data groups analyzed via one-way analysis of variance (ANOVA) and post hoc Bonferroni test. Single (*), double (**), and triple asterisks (***) indicate p-value less than 0.05, 0.01, and 0.001, respectively.

RESULTS

Fabrication and Characterization of BMV–CSC Patches.

Figure 1 illustrates the microfabrication and operation of BMV–CSC patches. The BMVs were endothelialized with HUVECs covering the luminal surface using a previously described microfluidic device based on three-dimensional hydrodynamic focusing. The resulting endothelialized microvessels had an inner and outer diameter of approximately 250 and 550 μm, respectively (Figure 1B), mimicking the structure of mammalian microvasculature.[11] The wall of the microfabricated BMVs consisted of biocompatible photo-crosslinked gelatin methacrylamide inter-penetrated with a network of FDA-approved poly(ethylene glycol). The extracellular scaffold of the BMVs was composed of

interconnected micropores including nanofibrous structure in the microvessel wall, as confirmed by scanning electron microscopy (Figure 1C). This unique structure supported the formation of a confluent endothelial cell layer covering the interior surface of the microvessel lumen (Figure 1B, right panel). Our previous studies showed that the BMV supports proper cellular behaviors including cell proliferation and endothelial cell–cell interaction.[11,12] Also, the BMV maintains its patent tubular morphology for at least 6 weeks after construction (Figure S1).

The BMV–CSC patch was created from encapsulating biaxially aligned endothelialized BMVs and hCSCs in a fibrin gel. After culturing the resulting patch for 8 days, the morphological analysis revealed that the luminal surface of the microfabricated microvessels was lined with confluent endothelial cells, while the hCSCs were external to the endothelialized microvessels in the surrounding fibrin matrix (Figure 1C, right panel). The biocompatible fibrin gel matrix supported cell retention and survival in the ischemic myocardium and mitigated immune rejection of the transplanted human cells. The endothelialized microvessels created channels between the hCSCs embedded in the patch and the surrounding tissue to facilitate nutrient transportation. The BMV–CSC patches released therapeutic factors to encourage the healing of scarred myocardial tissue post-MI injury (Figure 1D,E). We confirmed in our prior study that the CSC-secreted growth factors were sustainably released from the BMV–CSC patch as effectively as from the native cells culture for at least 14 days using enzyme-linked immunosorbent assay.[11]

BMV–CSC Patch Transplantation Improves Cardiac Function and Limits Pathological Remodeling After MI.

Inspired by the previous findings on the potency of microfabricated human endothelial microvessels to promote neovascularization both in vitro and in an ischemic rat heart,[11,13,17] we investigated whether therapy using the BMV–CSC patches could attenuate heart remodeling and improve cardiac pump function following ischemic injury in an athymic nude rat model of MI (Figure 2A). The acutely infarcted rat hearts were randomized to receive the BMV–CSC patch as well as three other control cardiac patches that include: (1) the HUVEC–CSC patch encapsulating a random mixture of HUVECs and hCSCs; (2) the CSC patch integrated with hCSCs only; and (3) the empty patch having no cells.

After treatment, the hearts were analyzed for fibrosis using Masson’s trichrome staining, where the fibrotic scar tissues are stained blue and the viable myocardium stained red. Figure 2B shows that the left ventricle wall of empty patch-treated rats was largely replaced by dense fibrotic tissue, similar to that in the rats that received no treatment after MI induction. The hearts treated with control cardiac patches (i.e., CSC patch and HUVEC–CSC patch) exhibited a trend of increasing viable tissue. Notably, the most viable myocardium was observed in the hearts that received BMV–CSC patches. Quantitative analysis showed that the MI-injured rats had viable myocardium that only covered 45 ± 5% of the infarct region (Figure 2C and Table S1). The HUVEC–CSC patch-treated hearts had improved myocardium viability of 58 ± 4%, significantly higher than those in the CSC patch-treated hearts (50 ± 3%) and the empty patch-treated hearts (47 ± 5%), respectively.

The BMV–CSC patch group exhibited the highest percentage of viable myocardium (70 ± 4%) in the infarct region among all of the patch-treated groups. Moreover, the wall thickening of the infarct area and the reduction of scar size were more evident in the BMV–CSC patch and HUVEC–CSC patch groups than observed in the CSC patch and empty patch groups (Figure 2D,E, and Table S1).

Echocardiography was performed 4 h post-MI induction on day 0 (baseline), day 14 (mid-point), and before animal euthanization on day 28 (end point). On day 0, the baseline left ventricular volumes at end-diastole (LVEDV) and end-systole (LVESV) were comparable across all treatment groups except the sham group; similar results were seen with the baseline left ventricular internal diameters at end-diastole (LVIDd) and end-systole (LVIDs), indicating that the surgical LAD occlusion created a comparable degree of initial injury across different groups of infarcted animals (Figure S2). The empty patch-recipient hearts showed a progressive decline in the left ventricular ejection fraction (LVEF) as well as the left ventricular fractional shortening (LVFS) over time, similar to those injured by MI surgery. The CSC patch and HUVEC–CSC patch treatments were able to augment the cardiac pump function within the initial 2 weeks; however, the augmentation was not sustained afterward (Figure S3). In contrast, the BMV–CSC patch therapy robustly boosted the LVEF as well as maintained the LVFS level over 4 weeks. At the end point, the hearts that received BMV–CSC patches had the highest LVEF level (60 ± 6%), which were 33 and 23% higher than those of the hearts that received the CSC and HUVEC–CSC patch therapies, respectively, although the function of the left ventricle did not fully recover to the normal level at the 4-week end point (Figure 3A,C, and Table S1). Further investigation of the treatment effect on ejection fraction (i.e., the change of LVEF at the 4-week end point relative to baseline) corroborated that the BMV–CSC patch therapy elicited the greatest reversal change in cardiac pump function (Figure 3D and Table S1). Furthermore, the recovery of both LVIDs and LVFS at the end point was more evident in the BMV–CSC patch treatment group than any other treatment group, which was translated into the greatest restoration of cardiac contractility in the hearts treated with the BMV–CSC patch (Figure 3E,H, and Table S1).

BMV–CSC Patch Transplantation Does Not Exacerbate Ventricular Arrhythmia and Pathological Cardiac Remodeling in a Porcine Model of Acute MI.

We further employed an experimental porcine MI model to assess the cardioprotective potency of BMV–CSC patch transplantation. We induced an acute myocardial ischemic injury in immunocompetent Yorkshire pigs (female, 8–10 weeks old, 20–30 kg) by distal occlusion of the LAD (Figure 4A). A BMV–CSC patch (5 cm × 5 cm × 1 mm, Figure S4) was transplanted over the infarcted region of a porcine heart. Control animals received HUVEC–CSC patch transplantation or no treatment post-MI induction. Electrocardiogram (ECG) records as well as blood and serum samples were collected pre-MI, 1 h, 24 h, 14 days, and 28 days post-MI, respectively. The ST-segment elevation from the lead II ECG signals and the increase in the blood level of cTnI 24 h post-LAD occlusion indicated successful induction of MI across different treatment groups (Figures 4B,D, and S5–S7). ECG analysis revealed that the control post-MI porcine hearts still had ST-segment elevation and the HUVEC–CSC patch-recipient hearts exhibited certain tachyarrhythmia (a fast heart

rate around 180 beats per minute compared to the baseline heart rate of around 130 beats per minute) at the end point, with a pathological Q wave indicating an old anterior wall MI.[18] Such abnormality disappeared in the BMV–CSC patch-treated animals except for the presence of minimal ST-segment depression, probably due to residual myocardial ischemia or nonischemic reasons such as hyperventilation (Figures S4–S6).[19,20] Future electrophysiologic study on the porcine hearts treated with the BMV–CSC patch in response to programmed electric stimulation could provide more information on the arrhythmogenic potential of the BMV–CSC patch therapy.

After the last echocardiography session at the 4-week end point, all animal hearts were harvested followed by slicing from the base to the apex for triphenyl tetrazolium chloride (TTC) staining to recognize the viable myocardial tissue (stained red) and the scar tissue (stained white). The macroscopic images of the TTC-stained heart slices indicated that the infarcted area of the BMV–CSC patch-recipient porcine hearts was relatively smaller on slices 3 and 4 compared to those of the HUVEC–CSC patch-recipient hearts or the MI-injured control hearts (Figure 4C,E; white, scar tissue; red, viable myocardium). Histological analysis using Masson's trichrome stain showed that both BMV–CSC and HUVEC–CSC patch therapies reduced myocardial fibrosis at the microscopic level. Furthermore, it was interesting to observe that fibrotic tissue was predominant in the host tissue interfaced with the implanted HUVEC–CSC patch at the 4-week end point, while sizable cardiac tissue was identified underneath the BMV–CSC patches (Figure S8). We reason that this attenuation in pathological ventricular remodeling was a result of the cardioprotective effect of the BMV–CSC patch, which is consistent with the morphometric analysis of the rat hearts that received different patch treatments.

BMV–CSC Patch Transplantation Does Not Induce Toxicity and Immunogenicity.

To assess the concerns for potential toxicity resulting from BMV–CSC patch transplantation, liver and kidney functions were evaluated with porcine blood samples collected at predetermined time intervals. We found that the animals that received BMV–CSC patch transplantation showed comparable liver enzyme levels over the 4 weeks (Figure S9A,B). These results indicated that BMV–CSC patch transplantation did not compromise the hepatic function. Furthermore, the blood urea nitrogen (BUN) and creatinine measurements confirmed that BMV–CSC patch transplantation did not impair renal function (Figure S9C,D).

We further evaluated the immunogenicity of BMV–CSC patch transplantation. The presence of trivial amounts of $CD3^+/CD8^+$ T cells, as well as $CD68^+$ macrophages in the porcine hearts that received different treatments (Figure S10), suggested that BMV–CSC patch transplantation was not associated with evident inflammation in the post-MI porcine heart. It should be noted that the fibrin gel used for patch fabrication is made of Tisseel, which has been approved by the FDA and has an endotoxin level of less than 0.5 EU mL^{-1}; the BMV is constructed using tissue culture grade materials and carefully maintained following aseptic technique guidelines. Therefore, the endotoxin burden of each BMV–CSC patch is estimated to be less than 0.0125 EU per patch (for rat study) or 1.25 EU per patch (for pig

study), which would unlikely contribute to cardiac inflammation in rats or pigs post-MI injury.

BMV–CSC Patch Transplantation Promotes Cardiac Function Recovery and Myocardial Regeneration in Post-MI Porcine Hearts.

Echocardiographic analysis over 4 weeks indicated that the porcine hearts that received the BMV–CSC patch showed a slight increase in cardiac contractility (measured by LVFS, Figure S11) but a marked cardiac pump function recovery (measured by LVEF, Figures 4F and S12) compared with the HUVEC–CSC or control groups. The calculation of treatment effects (defined as the difference between end point LVEF (or LVFS) and the baseline) indicates that while control group displayed a functional decline, the animals that received HUVEC–CSC or BMV–CSC patch therapy showed amelioration of cardiac contractile dysfunction post-MI; the animals treated with the BMV–CSC patch therapy showed the greatest restoration of cardiac pump function (Figures S10 and S11).

To validate whether the improvement in cardiac function after BMV–CSC patch transplantation was accompanied by myocardial regeneration, we first investigated the cardiomyocyte cycling at the 4-week end point via immunohistochemical staining for both α-SA and Ki67.[9,21] We found that BMV–CSC patch transplantation induced an evident increase in $Ki67^+$ cycling cardiomyocytes in the post-MI porcine heart relative to any other treatment (Figure S13). We further stained the hearts for two additional proliferation markers, i.e., pH3 (labeling cells in the late G2/M-phase) and AURKB (labeling cells in the cytokinesis phase).[3,22] At the 4-week end point, the localization of pH3 in the nuclei of non-cardiomyocytes or cardiomyocytes was more evident in the hearts after BMV–CSC patch transplantation than any other treatment group (Figure 5A). The elevated expression of AURKB within myocardial nuclei further confirmed the robust in vivo cardiomyocyte proliferation after BMV–CSC patch transplantation (Figure 5B), which contributed to the myogenesis in the post-MI heart.

BMV–CSC Patch Transplantation Enhances Endogenous Progenitor Cell Recruitment and Angiogenesis in the Peri-Infarct Region After MI.

To unravel the underlying mechanism of the therapeutic effects of BMV–CSC patch transplantation on acute MI, we first performed immunohistochemical analysis to detect Nkx2.5, a cardiac progenitor marker, in the infarcted heart. BMV–CSC patch transplantation remarkably upregulated the Nkx2.5 expression in the ischemic myocardium at the 4-week end point across all treatment groups (Figure 6A). It has been shown that the increase in the percentage of Nkx2.5 expression in cardiomyocytes facilitates the protection of cardiomyocytes from oxidative stress in the ischemic myocardium, which could aid cardiomyogenesis and heart repair.[23,24] Additionally, we noted a dramatic higher expression of CD34, a marker of endothelial progenitors, in the infarcted area of the porcine hearts that received BMV–CSC patch transplantation relative to other treatment groups (Figure S14).

To delineate the source of these CD34-positive cells, we further stained the hearts with porcine-specific CD34 and Flk-1 (an early marker of endothelial progenitors) simultaneously. The presence of $CD34^+$ $Flk\text{-}1^+$ (double-positive) cells was more evident in

the porcine hearts after BMV–CSC patch transplantation (Figure 6B), confirming that BMV–CSC patch therapy encouraged remarkable migration of endogenous bone marrow-derived endothelial progenitors to the injured heart 4 weeks post-treatment.[25,26] This recruitment was corroborated by the significant increase in the densities of both vWF^+ capillaries and α-SMA^+ arterioles found in the porcine hearts after BMV–CSC patch transplantation compared to other treatment groups (Figure 5C,D).[27,28]

BMV–CSC Patch Transplantation Suppresses Celluar Apoptosis and Inflammation in the Infarcted Porcine Hearts.

We further evaluated cell apoptosis in the scarred area across all animal groups (Figure 7A,C). BMV–CSC patch administration reduced the total $TUNEL^+$ apoptotic cells in the infarcted porcine hearts as much as the HUVEC–CSC patch did over the 4 weeks (Figure 7B). Further analysis via TUNEL assay combined with an α-SA co-stain indicated that the transplantation of BMV–CSC patch conferred the greatest protection of cardiomyocytes from apoptosis in the post-MI heart (Figure 7C).

To assess the in vivo anti-inflammatory ability of BMV–CSC patch therapy, we tracked the variation in the serum levels of several cytokines after different treatments over 4 weeks using ELISA. Previous preclinical and clinical studies have established that the post-MI hearts exhibit sustained elevation in levels of IL-1β, IL-6, and TNF-α that are expected to exacerbate myocardial inflammation during the acute MI phase (within 7 days).[29–34] Notably, both HUVEC–CSC and BMV–CSC patch transplantation limited the upregulation of these cytokines 24 h post-treatment. Furthermore, a remarkable IL-10 upregulation, which could alleviate inflammation, was observed in hearts that received BMV–CSC patch transplantation at the 4-week end point (Figure 7D,G). Together, these results suggest that functional benefits of the BMV–CSC patch therapy may be through activation of endogenous progenitor cells, promotion of neovascularization, attenuation of apoptosis, and suppression of proinflammatory cytokines.

DISCUSSION

The present study is the first to evaluate cardiac stromal cell patches integrated with microengineered biomimetic microvessels in experimental rodent and large animal MI models. It is well known that cardiac parenchymal and stromal cells function much better in the microenvironment with the coexistence of vasculature than that with the above cells only.[21,35–37] The vascularization of tissue-engineered constructs is attracting increasing interest in developing new microphysiological systems and translational medicine.[38,39] Employing a recently developed hydrodynamic focusing method to fabricate free-standing biomimetic microvessels over 1 m long and lined with endothelial cells, we constructed a vascularized cardiac patch. The vascularized patch could be easily constructed at appropriate sizes by encapsulating the biomimetic blood vessels together with hCSCs in a fibrin gel. Mounting evidence from preclinical and clinical studies has confirmed the beneficial effects of hCSCs in ischemic heart repair through paracrine signaling.[13] We and other research groups have extensively characterized the hCSCs in the past few years and found these cells rescue the ischemic myocardium via paracrine signaling rather than direct differentiation.

[13–15] We have also demonstrated the potential of multilineage differentiation from these cells; however, such differentiation events are rare.[16]

Our previous findings indicated that: (1) the microfabricated endothelialized microvessels mimicked the structure and function of capillaries; (2) the resulting BMV–CSC patch sustainably released paracrine factors comparable to the levels released during 7 days of coculture of native hCSCs and HUVECs; (3) after transplantation in the MI-injured rats for 4 weeks, BMV–CSC patch transplantation stimulated more profound angiogenesis and cardiomyogenesis in the peri-infarct region than conventional cardiac patches that encapsulate an equivalent concentration of hCSCs only or a mixture of equivalent numbers of HUVECs and hCSCs. In addition, we have assessed the integration of the BMV–CSC patch with host myocardium in MI-injured athymic nude rats in our prior work.[11] We observed persistent occurrence of vWF^+ blood vessel formation at the interface between the host tissue and the implanted BMV–CSC patch 4 weeks after transplantation. We also employed the immunostaining for both rat red blood cells and human endothelial cells and confirmed the perfusion of human microvessel lumen with host blood cells in the rat hearts after BMV–CSC patch transplantation, supporting the occurrence of anastomosis between patch microvessels and the host vasculature.[11] Together, the above findings indicated that our BMVs can integrate with the host vasculature to facilitate cardiac repair post-MI injury. In the present study, the treatment of infarcted rat hearts with BMV–CSC patches was linked to an increase in viable myocardium and infarct wall thickness as well as a decrease in scar size (Figure 2B,E). The attenuation of adverse cardiac remodeling was translated into cardiac function restoration in terms of both cardiac pump function and contractility of the hearts treated with the BMV–CSC patch (Figure 3).

Despite the widespread use of rodent models in preclinical cardiovascular research, the use of porcine models can provide more valuable insights into the pathophysiology of ischemic myocardium and implications of interventional therapies since pigs have more cardiovascular similarities to humans, in terms of anatomy, physiology, and size than the rodent species.[5,21–23] Thus, we were particularly curious to determine if the BMV–CSC patch therapy is efficacious and safe for treating MI-injured porcine hearts.

The BMV–CSC patch treatment did not increase the risk of ventricular arrhythmias in the infarcted porcine heart (Figure 4B). Moreover, the viable myocardial tissue was better preserved in the porcine hearts after BMV–CSC patch transplantation than those treated with the HUVEC–CSC patch (Figures 4C,E, and S8). The reduced pathological ventricular remodeling of BMV–CSC patch-treated animals was further demonstrated by the improvement in cardiac pump function compared with the HUVEC–CSC or control groups 4 weeks post-treatment (Figures 4F, S11 and S12). It has been reported that myocardial capillary networks surrounding resident cardiac cells, including cardiomyocytes, cardiac stromal cells, and progenitor cells, play a vital role in not only supplying oxygen and nutrients but also in regulating angiomyogenesis and tissue repair from myocardial injury.[36,40] The preorganized BMVs may provide such support to hCSCs more efficiently than is achieved simply by mixing the two cell types in the HUVEC–CSC patches, thereby promoting the CSC-mediated angiogenic signaling in cardioprotection.[41] Collectively, the paracrine mechanism and the microenvironment of the BMV–CSC patch contributed to the

augmented cardiac function relative to the HUVEC–CSC patch treatment, which is consistent with the results from the study in rats. It should be noted that in the immunocompetent pig model of MI, the case is somewhat different from that in the nude athymic rat infarct model. Any native human cells will likely be removed by the porcine immune system; this is in line with the fact that we did not find any perfused human microvessel with porcine blood cells via immunostaining in the porcine hearts after BMV–CSC patch transplantation (data not shown) as we did in the athymic rat counterparts,[11] suggesting that the integration of engineered human microvessels with the host vasculature did not occur. Therefore, in the injured immunocompetent porcine heart, our BMV–CSC patch exerted its therapeutic benefits mainly through protecting the encapsulated human cells from host immune attack[42–44] and enhancing the CSC-induced reparative paracrine signaling to rescue the infarcted myocardium.

BMV−CSC patch transplantation did not induce toxicity or aggravate inflammation in the infarcted heart of immunocompetent pigs. We reason that the biocompatibility of the BMV–CSC patch can be ascribed to the protective fibrin gel employed to encapsulate both BMVs and hCSCs. Fibrin has attracted increasing interests in bioscaffold fabrication for clinical applications owing to its excellent biocompatibility, biodegradability, and high cell seeding efficiency and adhesion ability.[10,23,45] Besides, it has been reported by us and many others that hCSCs maintain their in vivo viability and functionality after being encapsulated into fibrin or other biocompatible polymer patches.[9,11,46] In the present study, the fibrin gel matrix of the BMV–CSC patch not only avoided rejection of the transplanted cells but also supported the sustained release of therapeutic factors from the encapsulated hCSCs, thus contributing to the in vivo biocompatibility and bioactivity of the BMV–CSC patch. These results are consistent with our previous finding that polymeric nanogel-encapsulated hCSCs did not provoke host immune rejection but promoted angiomyogenesis in the MI-injured hearts of immunocompetent mice and pigs.[42] In addition, delivering cells encapsulated within an epicardial patch may alleviate the immunogenicity issue as compared to direct cell injection.[43,44] Therefore, we expect that the BMV–CSC patch will protect allogeneic cell transplants, which is favorable for its practical applications.

Our histological and immunohistochemical analyses confirmed that 4 weeks after MI injury, the viable myocardium and proliferating cardiac cells were remarkably compromised in animals from the MI group and that these reductions were prevented or reversed in the BMV–CSC patch-recipient animals, which was accompanied by an increase in $Nkx2.5^+$ cardiac progenitors and $CD34^+$ $Flk\text{-}1^+$ endothelial progenitors homing to the peri-infarct region. Collectively, these results are the first to suggest that the BMV–CSC patch therapy is safe and efficacious in restoring cardiac function, preserving cardiac morphometry, and recruiting endogenous progenitors to aid myocardial rescue after acute MI.

Further studies are needed to fully understand the reparative mechanisms of the BMV–CSC patch therapy before application to humans. First, there are likely different modes of action adopted in repairing the MI-damaged myocardium in animals with deficient versus healthy immune systems. A study design including additional immunocompetent rats or immunosuppressed pigs could provide a more complete analysis of the modes of action underlying the reparative benefits of the BMV–CSC patch therapy. Second, more

mechanistic studies (e.g., single-cell gene sequencing) are needed to analyze multiple cells in the hearts that receive BMV–CSC patch transplantation to define the mechanisms of repair.

CONCLUSIONS

In summary, our study represents the first to evaluate a microengineered biomimetic microvessel-integrated cardiac stromal cell patch for enhanced heart repair after ischemic injury. Current strategies of fabricating vascularized cardiac patches for ischemic heart repair are relatively cumbersome and not widely adopted in clinical practice. The BMV–CSC patch technology is developed to address this issue. Hydrodynamic focusing enables the fast (10 min) and facile fabrication of free-standing endothelialized microvessels that resemble mammalian vasculature. BMV–CSC patch transplantation facilitated the localization of therapeutic cells on the epicardial surface of the injured heart and created a protective microenvironment for the hCSCs to release regenerative factors to encourage cardiac repair. In the rat and pig models of acute MI, we demonstrated that the transplantation of a BMV–CSC patch significantly promoted cardiac function, reduced scar size, increased viable myocardial tissue, promoted neovascularization, and suppressed inflammation, showing enhanced therapeutic efficacy compared with other control patches. This work paves the way for future investigations to assess the translational value of the BMV–CSC patch therapy to rescue the ischemic heart and multiple ischemic tissues.

Recently, a novel human cardiac muscle patch (hCMP) containing human-induced pluripotent stem cell (hiPSC)-derived trilineage cardiac cells was delicately created with its electrophysiological and contractile properties resembling those of native myocardial tissue. The hCMP promoted recovery of the post-MI porcine hearts through considerable engraftment of engineered cardiac muscle with enhanced maturation and exosome-mediated paracrine signaling.[21] Of note, in the present study, we took a different strategy to integrate preformed, microengineered, biomimetic microvessels with hCSCs in a biological scaffold to create a “vessel-in-parenchyma” microenvironment that could enhance the hCSC-induced reparative paracrine signaling in infarct healing. Cardiac patches are still being actively explored as a promising option to effectively deliver cell therapy to the site of MI injury despite the surgical procedures that are often required for patch deployment. We envision that advanced, minimally invasive approaches could reduce the injury associated with BMV–CSC patch delivery. Future studies could focus on the design of a smart BMV–CSC patch that dynamically modulates the reparative paracrine signaling in response to the pathological microenvironment for the delicate repair of the post-MI heart.

Supplementary Material

Refer to Web version on PubMed Central for supplementary material.

ACKNOWLEDGMENTS

This work was supported by the grants from the National Institutes of Health under award numbers R01 HL123920, HL137093, HL144002, HL149940, HL147357, and HL146153 to K.C., from American Heart Association under award numbers 18TPA34230092 and 19EIA34660286 to K.C. and award number 18TPA34230031 to M.A.D., from National Science Foundation under award number EEC-1160483 to M.A.D. through the Nanosystems Engineering

Research Center for Advanced Self-Powered Systems of Integrated Sensors and Technologies (ASSIST), from North Carolina State University Chancellor's Innovation Fund to K.C. and UNC General Assembly Research Opportunities Initiative award to K.C. and F.S.L. This work was performed in part at the Analytical Instrumentation Facility (AIF) at North Carolina State University, which is supported by the State of North Carolina and the National Science Foundation (ECCS-1542015). The AIF is a member of the North Carolina Research Triangle Nanotechnology Network (RTNN), a site in the National Nanotechnology Coordinated Infrastructure (NNCI).

REFERENCES

(1). Prabhu SD; Frangogiannis NG The Biological Basis for Cardiac Repair After Myocardial Infarction. Circ. Res 2016, 119, 91–112. [PubMed: 27340270]

(2). Dick SA; Macklin JA; Nejat S; Momen A; Clemente-Casares X; Althagafi MG; Chen J; Kantores C; Hosseinzadeh S; Aronoff L; Wong A Self-renewing resident cardiac macrophages limit adverse remodeling following myocardial infarction. Nat. Immunol 2019, 20, 29–39. [PubMed: 30538339]

(3). Su T; Huang K; Ma H; Liang H; Dinh PU; Chen J; Shen D; Allen TA; Qiao L; Li Z; Hu S; Cores J; Frame BN; Young AT; Yin Q; Liu J; Qian L; Caranasos TG; Brudno Y; Ligler FS; Cheng K Platelet-inspired nanocells for targeted heart repair after ischemia/reperfusion injury. Adv. Funct. Mater 2019, 29, No. 1803567.

(4). Park SJ; Kim RY; Park BW; Lee S; Choi SW; Park JH; Choi JJ; Kim SW; Jang J; Cho DW; Chung HM; Moon SH; Ban K; Park HJ Dual stem cell therapy synergistically improves cardiac function and vascular regeneration following myocardial infarction. Nat. Commun 2019, 10, No. 3123.

(5). Tang J; Su T; Huang K; Dinh PU; Wang Z; Vandergriff A; Hensley MT; Cores J; Allen T; Li T; Sproul E; Mihalko E; Lobo LJ; Ruterbories L; Lynch A; Brown A; Caranasos TG; Shen D; Stouffer GA; Gu Z; Zhang J; Cheng K Targeted repair of heart injury by stem cells fused with platelet nanovesicles. Nat. Biomed. Eng 2018, 2, 17–26. [PubMed: 29862136]

(6). Tompkins BA; Balkan W; Winkler J; Gyöngyösi M; Goliasch G; Fernández-Avilés F; Hare JM Preclinical studies of stem cell therapy for heart disease. Circ. Res 2018, 122, 1006–1020. [PubMed: 29599277]

(7). Matsa E; Burridge PW; Wu JC Human stem cells for modeling heart disease and for drug discovery. Sci. Transl. Med 2014, 6, No. 239ps6.

(8). Gao L; Kupfer ME; Jung JP; Yang L; Zhang P; Da Sie Y; Tran Q; Ajeti V; Freeman BT; Fast VG; Campagnola PJ; Ogle BM; Zhang JY Myocardial tissue engineering with cells derived from human-induced pluripotent stem cells and a native-like, high-resolution, 3-dimensionally printed scaffold. Circ. Res 2017, 120, 1318–1325. [PubMed: 28069694]

(9). Tang J; Wang J; Huang K; Ye Y; Su T; Qiao L; Hensley MT; Caranasos TG; Zhang J; Gu Z; Cheng K Cardiac cell–integrated microneedle patch for treating myocardial infarction. Sci. Adv 2018, 4, No. eaat9365.

(10). Riemenschneider SB; Mattia DJ; Wendel JS; Schaefer JA; Ye L; Guzman PA; Tranquillo RT Inosculation and perfusion of pre-vascularized tissue patches containing aligned human microvessels after myocardial infarction. Biomaterials 2016, 97, 51–61. [PubMed: 27162074]

(11). Su T; Huang K; Daniele MA; Hensley MT; Young AT; Tang J; Allen TA; Vandergriff AC; Erb PD; Ligler FS; Cheng K Cardiac stem cell patch integrated with microengineered blood vessels promotes cardiomyocyte proliferation and neovascularization after acute myocardial infarction. ACS Appl. Mater. Interfaces 2018, 10, 33088–33096. [PubMed: 30188113]

(12). DiVito KA; Daniele MA; Roberts SA; Ligler FS; Adams AA Microfabricated blood vessels undergo neoangiogenesis. Biomaterials 2017, 138, 142–152. [PubMed: 28570946]

(13). Li TS; Cheng K; Malliaras K; Smith RR; Zhang Y; Sun B; Matsushita N; Blusztajn A; Terrovitis J; Kusuoka H; Marbán L; Marbán E Direct comparison of different stem cell types and subpopulations reveals superior paracrine potency and myocardial repair efficacy with cardiosphere-derived cells. J. Am. Coll. Cardiol 2012, 59, 942–953. [PubMed: 22381431]

(14). Malliaras K; Li TS; Luthringer D; Terrovitis J; Cheng K; Chakravarty T; Galang G; Zhang Y; Schoenhoff F; Van Eyk J; Marbán L Safety and efficacy of allogeneic cell therapy in infarcted rats transplanted with mismatched cardiosphere-derived cells. Circulation 2012, 125, 100–112. [PubMed: 22086878]

(15). Tang J; Shen D; Caranasos TG; Wang Z; Vandergriff AC; Allen TA; Hensley MT; Dinh PU; Cores J; Li TS; Zhang J; Kan Q; Cheng K Therapeutic microparticles functionalized with biomimetic cardiac stem cell membranes and secretome. Nat. Commun 2017, 8, No. 13724.

(16). Cheng K; Ibrahim A; Hensley MT; Shen D; Sun B; Middleton R; Liu W; Smith RR; Marbán E Relative roles of CD 90 and c-Kit to the regenerative efficacy of cardiosphere-derived cells in humans and in a mouse model of myocardial infarction. J. Am. Heart Assoc 2014, 3, No. e001260.

(17). Adams AA; Daniele MA; Ligler FS Micro Blood Vessels and Tissue Ducts. U.S. Patent US10,208,289 B22019.

(18). Haiat R; Chiche P Transient abnormal Q waves in the course of ischemic heart disease. Chest 1974, 65, 140–144. [PubMed: 4810671]

(19). Savonitto S; Cohen MG; Politi A; Hudson MP; Kong DF; Huang Y; Pieper KS; Mauri F; Wagner GS; Califf RM; Topol EJ; Granger CB Extent of ST-segment depression and cardiac events in non-ST-segment elevation acute coronary syndromes. Eur. Heart J 2005, 26, 2106–2113. [PubMed: 15987706]

(20). Chen CC; Chen SA; Tai CT; Kuo TBJ; Chang MS; Prystowsky EN Hyperventilation facilitates induction of supraventricular tachycardia: a novel method and the possible mechanism. J. Cardiovasc. Electrophysiol 2001, 12, 1242–1246. [PubMed: 11761410]

(21). Gao L; Gregorich ZR; Zhu WQ; Mattapally S; Oduk Y; Lou X; Kannappan R; Borovjagin AV; Walcott GP; Pollard AE; Fast VG; Hu XY; Lloyd SG; Ge Y; Zhang JY Large cardiac muscle patches engineered from human induced-pluripotent stem cell-derived cardiac cells improve recovery from myocardial infarction in swine. Circulation 2018, 137, 1712–1730. [PubMed: 29233823]

(22). Zhu WQ; Zhang E; Zhao M; Chong ZC; Fan CM; Tang YW; Hunter JD; Borovjagin AV; Walcott GP; Chen JY; Qin GJ; Zhang JY Regenerative potential of neonatal porcine hearts. Circulation 2018, 138, 2809–2816. [PubMed: 30030418]

(23). Ye L; Chang YH; Xiong Q; Zhang P; Zhang L; Somasundaram P; Lepley M; Swingen C; Su L; Wendel JS; Guo J; Jang A; Rosenbush D; Greder L; Dutton JR; Zhang JH; Kamp TJ; Kaufman DS; Ge Y; Zhang JY Cardiac repair in a porcine model of acute myocardial infarction with human induced pluripotent stem cell-derived cardiovascular cells. Cell Stem Cell 2014, 15, 750–761. [PubMed: 25479750]

(24). Chen WP; Liu YH; Ho YJ; Wu SM Pharmacological inhibition of TGFβ receptor improves Nkx2.5 cardiomyoblast-mediated regeneration. Cardiovasc. Res 2015, 105, 44–54. [PubMed: 25362681]

(25). Heeschen C; Aicher A; Lehmann R; Fichtlscherer S; Vasa M; Urbich C; Mildner-Rihm C; Martin H; Zeiher AM; Dimmeler S Erythropoietin is a potent physiologic stimulus for endothelial progenitor cell mobilization. Blood 2003, 102, 1340–1346. [PubMed: 12702503]

(26). Morrone D; Felice F; Scatena C; De Martino A; Picoi MLE; Mancini N; Blasi S; Menicagli M; Di Stefano R; Bortolotti U; Naccarato AG; Balbarini A Role of circulating endothelial progenitor cells in the reparative mechanisms of stable ischemic myocardium. Int. J. Cardiol 2018, 257, 243–246. [PubMed: 28918896]

(27). Ashammakhi N; Ahadian S; Darabi MA; El Tahchi M; Lee J; Suthiwanich K; Sheikhi A; Dokmeci MR; Oklu R; Khademhosseini A Minimally invasive and regenerative therapeutics. Adv. Mater 2019, 31, No. 1804041.

(28). Redd MA; Zeinstra N; Qin W; Wei W; Martinson A; Wang Y; Wang RK; Murry CE; Zheng Y Patterned human microvascular grafts enable rapid vascularization and increase perfusion in infarcted rat hearts. Nat. Commun 2019, 10, No. 584.

(29). Gabriel AS; Martinsson A; Wretlind B; Ahnve S IL-6 levels in acute and post myocardial infarction: their relation to CRP levels, infarction size, left ventricular systolic function, and heart failure. *Eur.* J. Intern. Med 2004, 15, 523–528.

(30). Nian M; Lee P; Khaper N; Liu P Inflammatory cytokines and postmyocardial infarction remodeling. Circ. Res 2004, 94, 1543–1553. [PubMed: 15217919]

(31). Xu S; Xu X; Guo Y; Gao W Inflammatory responses after intracoronary mononuclear BM cell therapy in swine. Bone Marrow Transplant 2009, 44, 427–431. [PubMed: 19333231]

(32). Chen ZW; Qian JY; Ma JY; Chang SF; Yun H; Jin H; Sun AJ; Zou YZ; Ge JB TNF-α-induced cardiomyocyte apoptosis contributes to cardiac dysfunction after coronary micro-embolization in mini-pigs. J. Cell. Mol. Med 2014, 18, 1953–1963. [PubMed: 25130514]

(33). Kaza AK; Wamala I; Friehs I; Kuebler JD; Rathod RH; Berra I; Ericsson M; Yao R; Thedsanamoorthy JK; Zurakowski D; Levitsky S Myocardial rescue with autologous mitochondrial transplantation in a porcine model of ischemia/reperfusion. J. Thorac. Cardiovasc. Surg 2017, 153, 934–943. [PubMed: 27938904]

(34). Van Hout GP; Bosch L; Ellenbroek GH; De Haan JJ; Van Solinge WW; Cooper MA; Arslan F; De Jager SC; Robertson AA; Pasterkamp G; Hoefer IE The selective NLRP3-inflammasome inhibitor MCC950 reduces infarct size and preserves cardiac function in a pig model of myocardial infarction. Eur. Heart J 2016, 38, 828–836.

(35). Schoenebeck JJ; Keegan BR; Yelon D Vessel and blood specification override cardiac potential in anterior mesoderm. Dev. Cell 2007, 13, 254–267. [PubMed: 17681136]

(36). Go´mez-Gaviro MV; Lovell-Badge R; Ferna´ndez-Avile´s F; Lara-Pezzi E The vascular stem cell niche. J. Cardiovasc. Transl. Res 2012, 5, 618–630. [PubMed: 22644724]

(37). Chiu LL; Montgomery M; Liang Y; Liu H; Radisic M Perfusable branching microvessel bed for vascularization of engineered tissues. Proc. Natl. Acad. Sci. U.S.A 2012, 109, E3414–E3423. [PubMed: 23184971]

(38). Zhang B; Montgomery M; Chamberlain MD; Ogawa S; Korolj A; Pahnke A; Wells LA; Massé S; Kim J; Reis L; Momen A; Nunes SS; Wheeler AR; Nanthakumar K; Keller G; Sefton MV; Radisic M Biodegradable scaffold with built-in vasculature for organ-on-a-chip engineering and direct surgical anastomosis. Nat. Mater 2016, 15, 669–678. [PubMed: 26950595]

(39). Fleischer S; Tavakol DN; Vunjak-Novakovic G From Arteries to Capillaries: Approaches to Engineering Human Vasculature. Adv. Funct. Mater 2020, 30, No. 1910811.

(40). Gray GA; Toor IS; Castellan RF; Crisan M; Meloni M Resident cells of the myocardium: more than spectators in cardiac injury, repair and regeneration. Curr. Opin. Physiol 2018, 1, 46–51. [PubMed: 29876531]

(41). Aguirre A; Planell JA; Engel E Dynamics of bone marrow-derived endothelial progenitor cell/mesenchymal stem cell interaction in co-culture and its implications in angiogenesis. Biochem. Biophys. Res. Commun 2010, 400, 284–291. [PubMed: 20732306]

(42). Tang J; Cui X; Caranasos TG; Hensley MT; Vandergriff AC; Hartanto Y; Shen D; Zhang H; Zhang J; Cheng K Heart repair using nanogel-encapsulated human cardiac stem cells in mice and pigs with myocardial infarction. ACS Nano 2017, 11, 9738–9749. [PubMed: 28929735]

(43). Levit RD; Landázuri N; Phelps EA; Brown ME; García AJ; Davis ME; Joseph G; Long R; Safley SA; Suever JD; Lyle AN Cellular encapsulation enhances cardiac repair. J. Am. Heart Assoc 2013, 2, No. e000367.

(44). Burdick JA; Mauck RL; Gerecht S To serve and protect: hydrogels to improve stem cell-based therapies. Cell Stem Cell 2016, 18, 13–15. [PubMed: 26748751]

(45). Higuchi A; Ku NJ; Tseng YC; Pan CH; Li HF; Kumar SS; Ling QD; Chang Y; Alarfaj AA; Munusamy MA; Benelli G; et al. Stem cell therapies for myocardial infarction in clinical trials: bioengineering and biomaterial aspects. Lab. Invest 2017, 97, 1167–1179. [PubMed: 28869589]

(46). Kim DH; Smith RR; Kim P; Ahn EH; Kim HN; Marbán E; Suh KY; Levchenko A; et al. Nanopatterned cardiac cell patches promote stem cell niche formation and myocardial regeneration. Integr. Biol 2012, 4, 1019–1033.

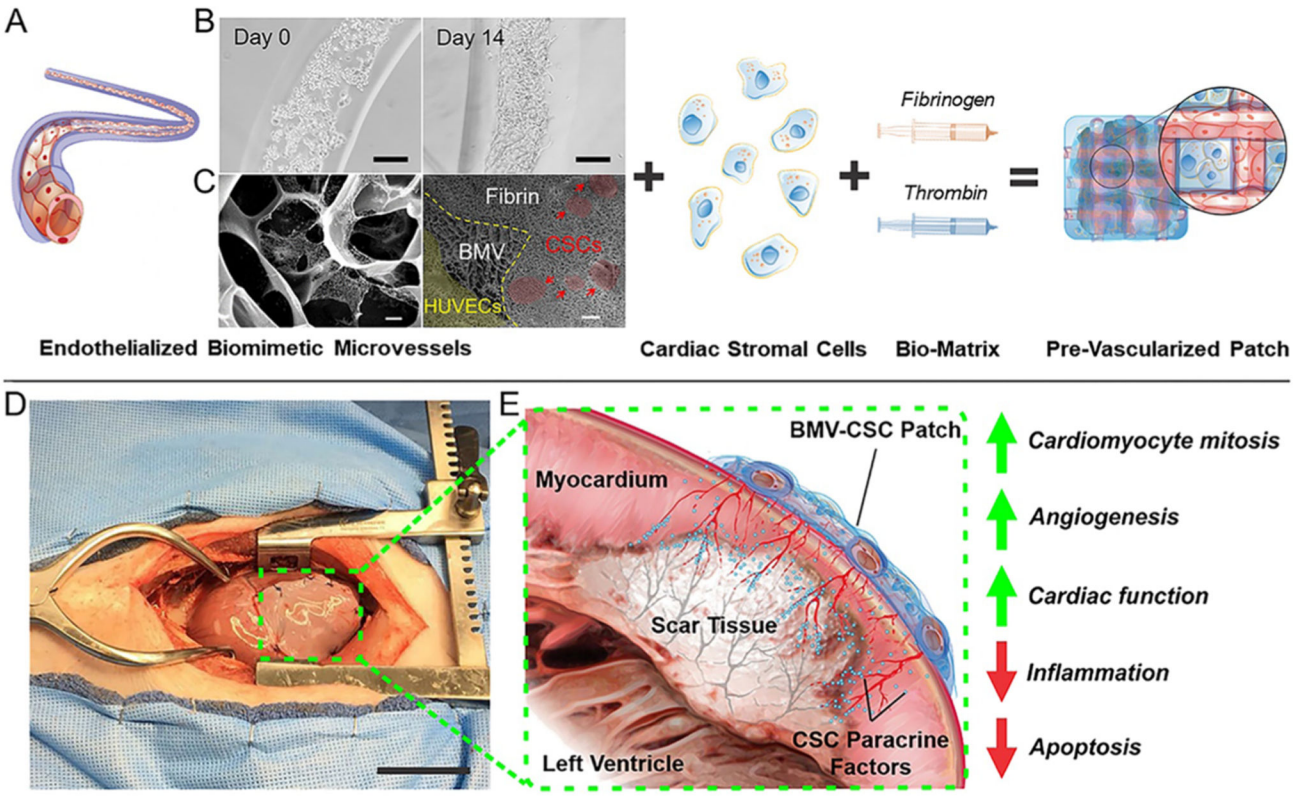

Figure 1.

Fabrication of cardiac cell patch integrated with engineered biaxial blood vessel network and treatment of myocardial infarction. (A) Endothelialized biomimetic microvessels are fabricated separately using hydrodynamic focusing techniques, then combined with hCSCs in a 3D fibrin matrix to form a cardiac cell patch with an organized blood vessel network. (B) Optical micrographs of human endothelial cells forming a coherent luminal lining within the microvessels over 14 days of culture. (C) Electron micrographs revealing the morphology of the 3D matrix of the BMV and the BMV–CSC patch after 8 days of in vitro culture. The red and yellow areas denote the hCSCs and the HUVECs in the microvessel lumen, respectively. (D) Photograph of the BMV–CSC patch transplanted onto porcine heart after MI. (E) Illustration of heart cross-section after MI and transplant of the BMV–CSC patch. The patch transplantation onto the infarcted region of a porcine heart results in therapeutic effects from both integration and paracrine signaling, including angiogenesis, the improvement of cardiac function, and mitigation of pathological tissue remodeling. Scale bars, (B) 100 μm; (C) Left: 1 μm; Right: 10 μm; (D) 5 cm.

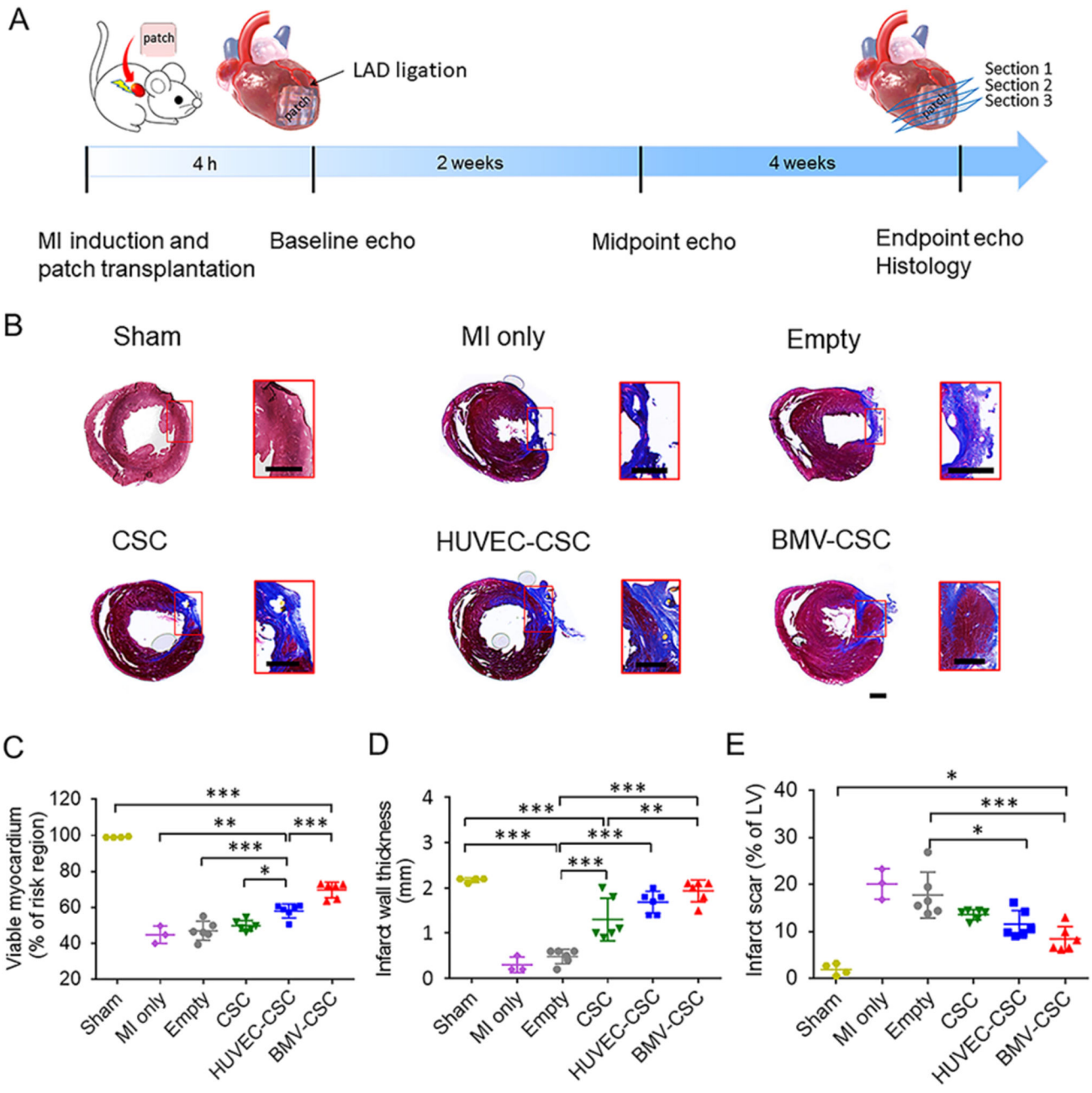

Figure 2.

BMV–CSC patch therapy ameliorated pathological cardiac remodeling in the post-MI rat heart. (A) Overall study design. (B) Detection of necrotic (blue) and viable (red) myocardium in rat hearts across different treatment groups at the 4-week end point using Masson's trichrome staining. Red squares indicate high magnification images. The percentage of viable tissue (C), infarct wall thickness (D), and the percentage of infarct tissue (E) were quantified according to the Masson's trichrome stain. Scale bar, 1 mm.

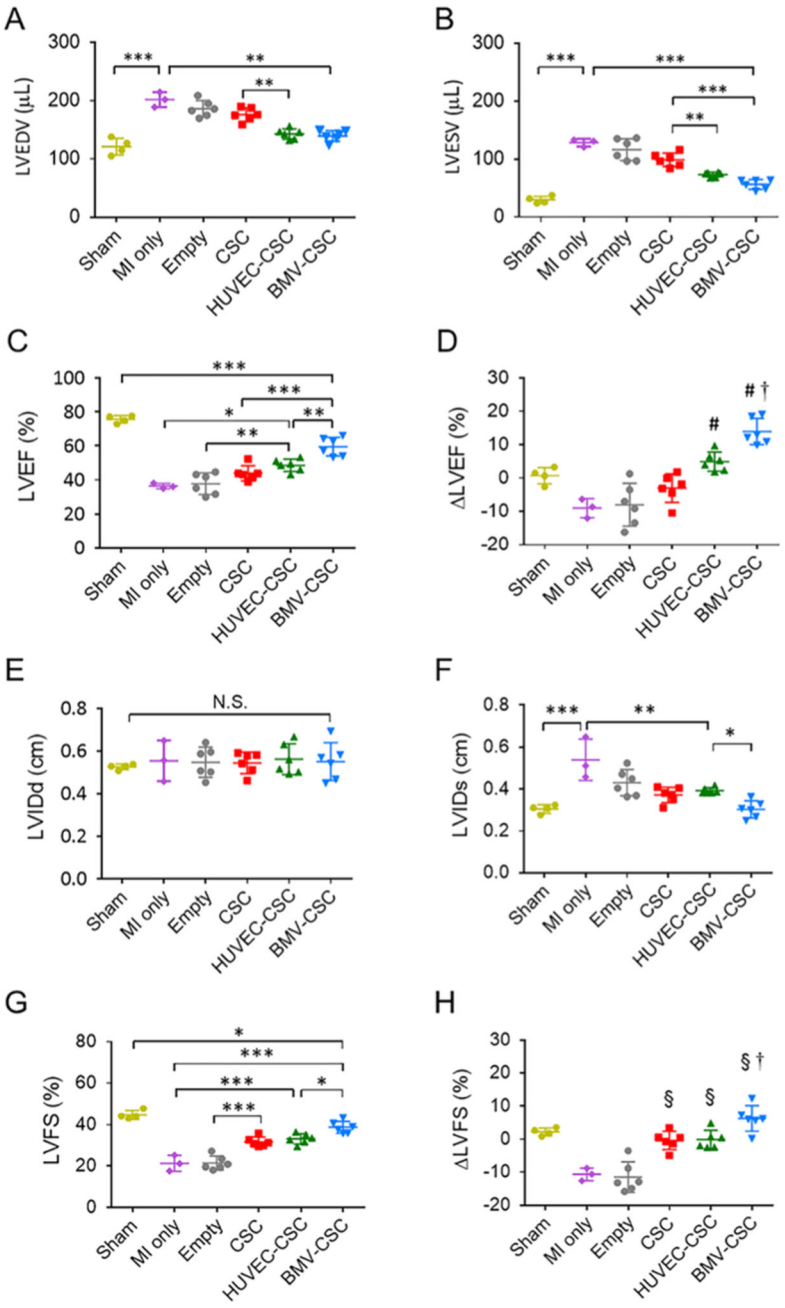

Figure 3.

BMV–CSC patch therapy improved cardiac function following acute MI. Echocardiographic assessment of (A) LVEDV, (B) LVESV, and (C) LVEF at the 4-week end point in rats that received different treatments. (D) LVEF change between the 4-week end point and the baseline. # denotes a *p*-value less than 0.05 when compared to MI-only, empty patch, or CSC patch group; † denotes a *p*-value less than 0.05 when compared to all other groups. (E) LVIDd, (F) LVIDs, and (G) LVFS measured by echocardiography at the 4-week end point in rats that received different treatments. (H) LVFS change at the 4-week end point relative to

the baseline. § denotes a *p*-value of less than 0.05 when compared to the MI-only or empty patch group; † denotes a *p*-value of less than 0.05 when compared to all other groups.

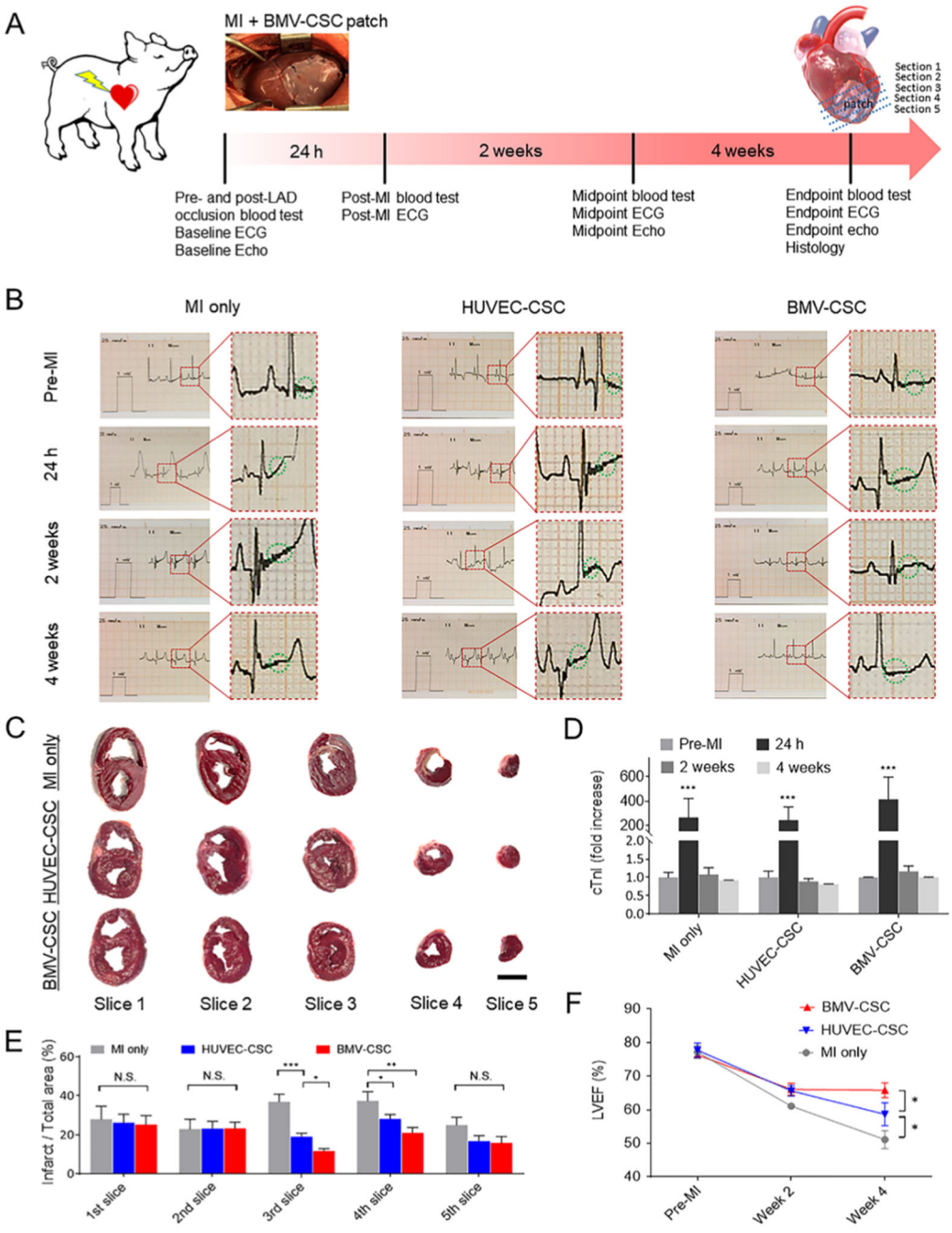

Figure 4.

Functional benefits of the BMV–CSC patch therapy in post-MI porcine hearts. (A) Overall study design. The porcine MI was inducted via LAD occlusion followed by BMV–CSC patch transplantation. (B) Lead II ECGs were collected at pre-MI, 24 h, 2 weeks, and 4 weeks post-MI from different treatment groups ($n = 3$). The green dashed circle indicates ST-segment. (C) Macroscopic images of TTC-stained heart slices (from the base to the apex of an individual heart in 1 cm thickness) of the porcine hearts that received different treatments at the 4-week end point. The white area denotes myocardial scar tissue. (D) Blood level of cTnI was measured pre-MI, 24 h, 2 weeks, and 4 weeks post-MI in each

treatment group. (E) Quantification of the percentage of infarction area in heart slices using ImageJ software. (F) Trajectory showing the change in LVEF determined by the echocardiography of the porcine hearts with different treatments over the 4-week time course. Scale bar, 3 cm.

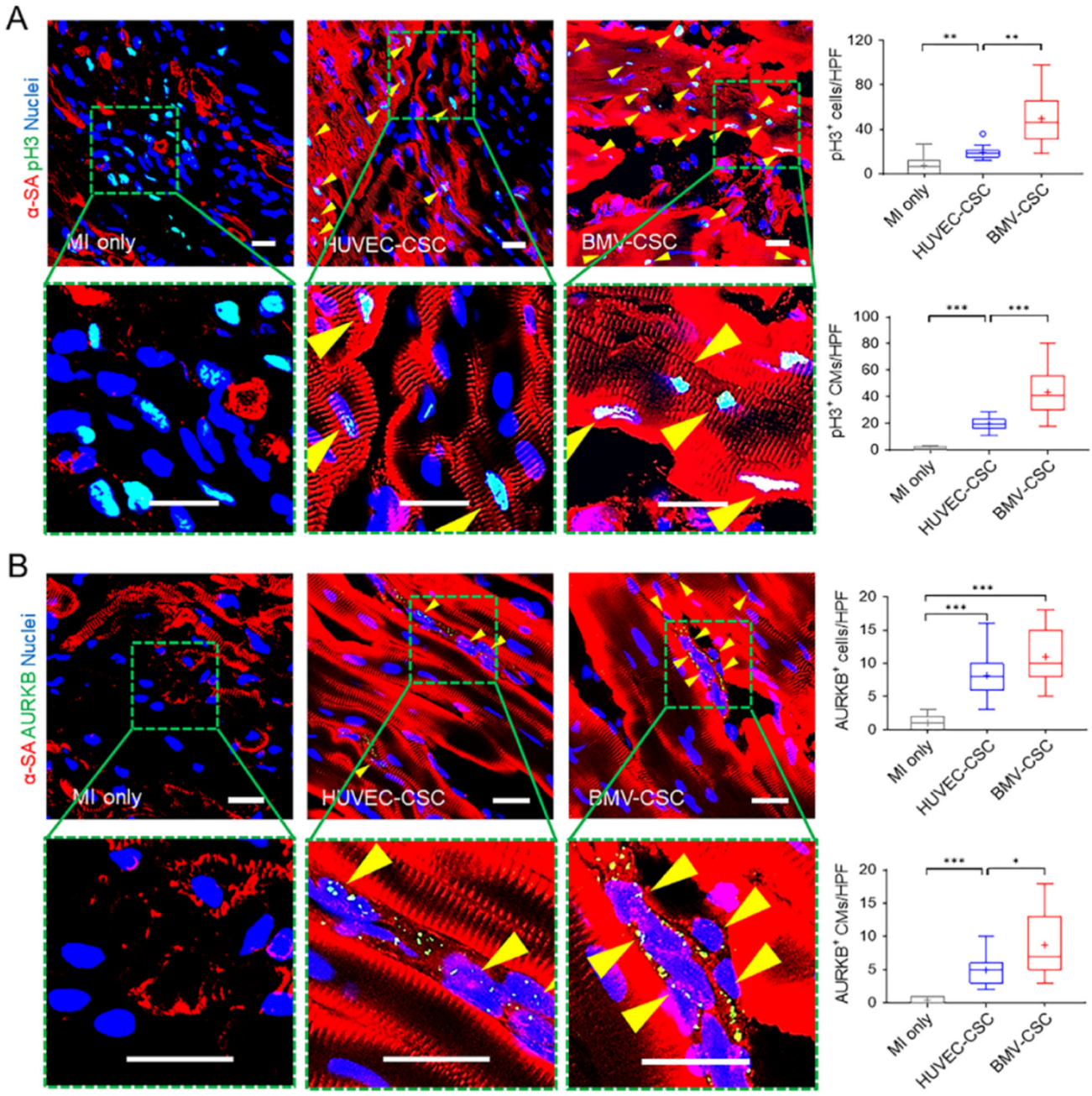

Figure 5.

BMV–CSC patch therapy promoted cardiomyocyte mitotic activity in the post-MI porcine heart. (A) Presence of $pH3^+$ cardiomyocytes ($pH3^+$ α-SA^+ double-positive cells; yellow arrowheads) in the infarcted area across different treatment groups at week 4. Quantification shows total $pH3^+$ cells as well as $pH3^+$ cardiomyocytes in different groups. (B) Presence of $AURKB^+$ cardiomyocytes (yellow arrowheads) in the infarcted area across different treatment groups at week 4. Quantification shows total $AURKB^+$ cells as well as $AURKB^+$ cardiomyocytes in different groups ($n = 3$). Scale bars, 20 μm.

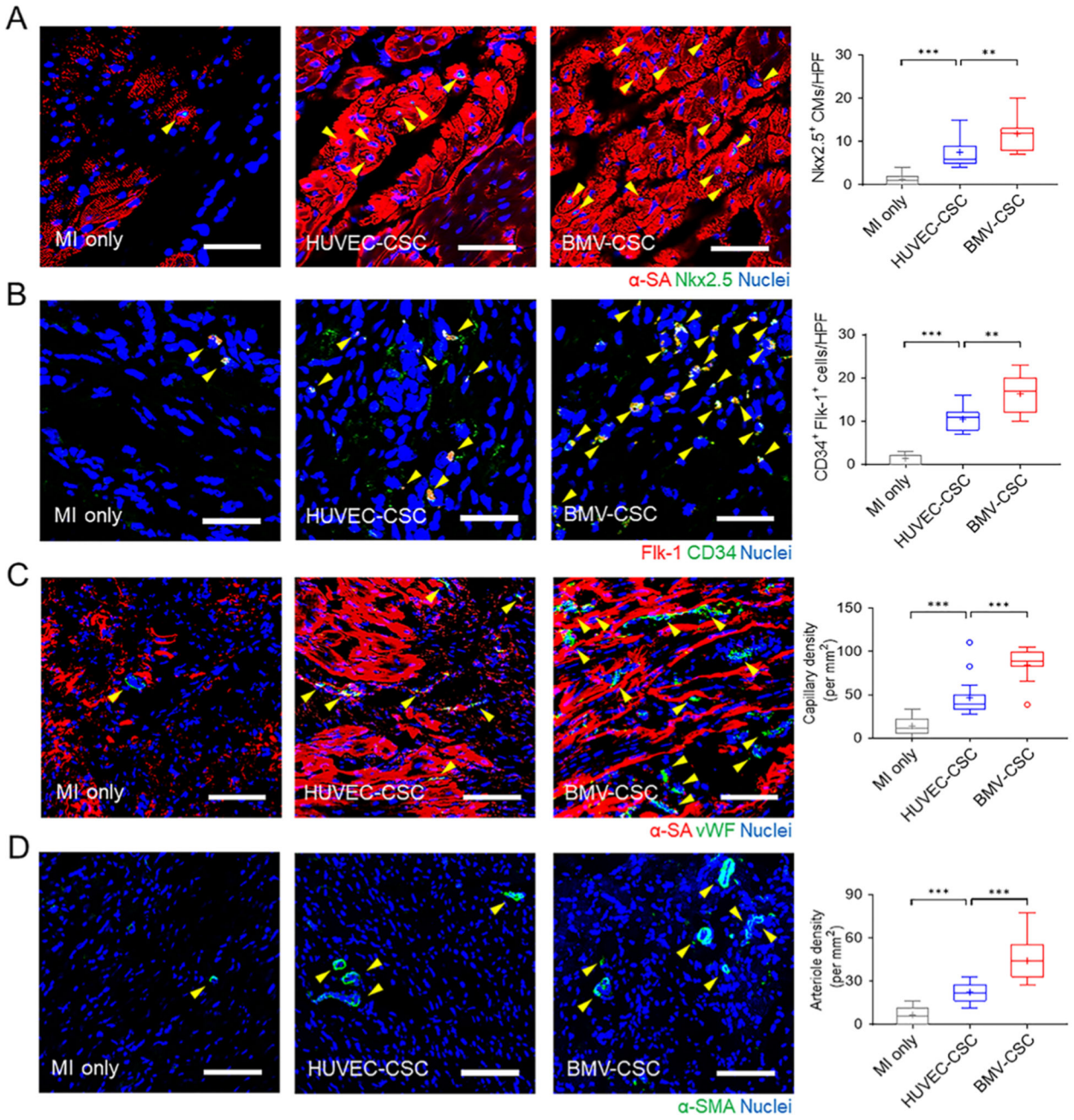

Figure 6.

BMV–CSC patch therapy promoted endogenous repair after acute MI. (A–D) Presence of Nkx2.5$^+$ cardiomyocytes (A), CD34$^+$ Flk-1$^+$ (double-positive) cells (B), vWF$^+$ capillaries (C), and α-SMA$^+$ arterioles in the peri-infarct region across different treatment groups at week 4. A positive stain is indicated by a yellow arrowhead. The number of Nkx2.5$^+$ cardiomyocytes, CD34$^+$ Flk-1$^+$ (double-positive) cells, vWF$^+$ capillary density, or α-SMA$^+$ arteriole density is quantified using ImageJ software. Scale bars, (A, B) 50 μm; (C, D) 100 μm.

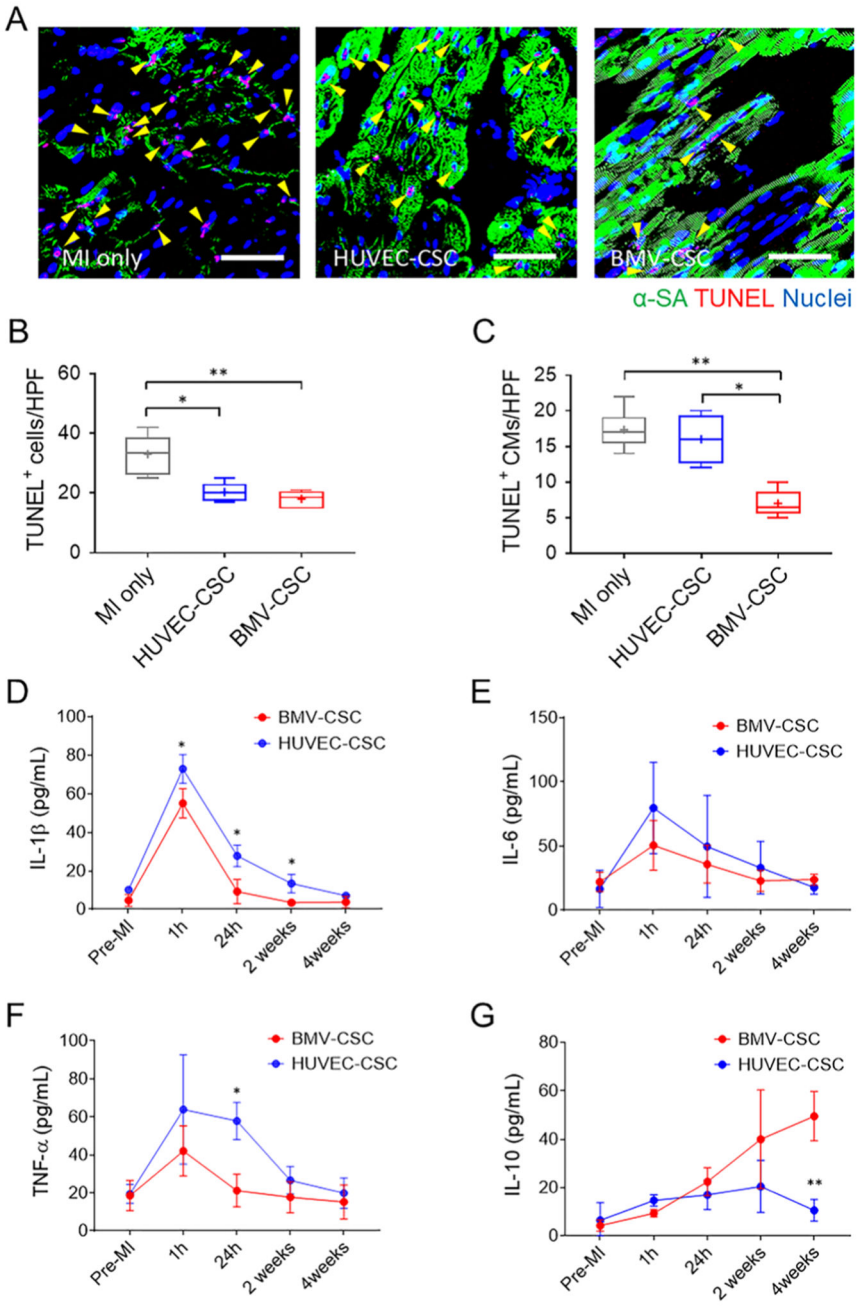

Figure 7.

BMV–CSC Patch Therapy Suppressed Celluar Apoptosis and Inflammation in the Infarcted Porcine Hearts. (A) Presence of TUNEL$^+$ cells in the infarcted porcine hearts across different treatment groups ($n = 3$) at the 4-week end point. Yellow arrowheads indicate TUNEL-positive cardiomyocytes. Quantification of TUNEL$^+$ cells (B) and TUNEL$^+$ cardiomyocytes (C) are performed using ImageJ software. Scale bars, 50 μm. (D–G) Porcine serum levels of IL-1β (D), IL-6 (E), TNF-α (F), and IL-10 (G) measured pre-MI, 1 h, 24 h, 2 weeks, and 4 weeks after different patch treatments, respectively. In comparison, the

reference porcine serum levels of IL-1β, IL-6, and TNF-α within the first 2 weeks post-MI maintain at 100–200, 40–419, 65–80 pg mL^{-1}, respectively.[28–31]